ACP Response to RC3 for *Low Temperature Ice Nucleation of Sea Spray and Secondary Marine Aerosols under Cirrus Cloud Conditions*
Format: The reviewers' comments are quoted in italics
Line number in the response refers to the revised manuscript with tracked changes Quotation in red color stands for revised/added text in the revised manuscript
Responses in blue

Patnaude et al. characterized the formation of ice nucleating particles in primary sea spray aerosols (pSSA), secondary marine aerosols (SMA), and a mixture of oxidized SSA and SMA generated in a marine aerosol reference tank and exposed to hydroxyl radicals in an oxidation flow reactor. They concluded that heterogenous ice nucleation occurred with pSSA, homogenous ice nucleation occurred with SMA, and that the INP formation potentials of aSSA + SMA and pSSA were similar.

Comments

In the abstract (L16-L18), based on results presented later in the paper, the authors state: "Similarities between freezing behaviors of the pSSA and aSSA+SMA at all temperatures suggest atmospheric aging has little effect on the heterogeneous freezing behavior of SSA at these cirrus temperatures and remains dominated by the crystalline salts." I think this conclusion is flawed the way it is presented. It might be applicable to the specific experimental conditions used in this manuscript, but it seems unlikely to me that it can be generalized to other SSA and SMA. First, I couldn't find any characterization of organic content in the pSSA generated here. It seems plausible to me that the MART-generated pSSA could be relatively inert simply because it has negligible organic content, whereas pSSA with higher organic content might be more reactive towards OH and therefore experience greater changes in IN formation potential. Second, no concrete evidence of SMA coating the pSSA or aSSA was provided - as the authors pointed out, the specific conditions that were used strongly favored homogenous nucleation of SMA over condensation of SMA onto SSA. They note that "the higher concentration of aSSA+SMA compared to pSSA from natural SW between 200 nm and 1 μm (Figure 2b) suggests some modification of the pSSA" but there is no way to prove that this is associated with gas-phase condensation over the other possible explanations that were provided (L172-L174). If it were due to condensation, the aSSA+SMA size distribution should be shifted towards larger particle sizes rather than a higher concentration of the same size particles. I interpreted Figure 2b to suggest that there is negligible condensed SMA on the SSA. Third, because this paper demonstrates that the IN formation efficiency of SMA is clearly lower than that of SSA, a mixed aSSA+SMA particle should at some threshold SMA:SSA ratio have lower IN formation potential than pure SSA particles. I don't know what that ratio is, but it doesn't seem to me that it was reached here. Overall, it seems valid to conclude that SMA doesn't form INP as efficiently as SSA, and that the IN formation efficiency of these pSSA didn't change appreciably following OH exposure, but I don't think any sort of definitive conclusions can be made regarding the IN formation efficiency of mixed SSA/SMA particles or of other pSSA particles that might contain more organics.

We thank the reviewer for the thorough read and for the many helpful suggestions, which we have carefully considered. Below, we respond to the various comments.

With regard to the comments on the lack of characterization of organic content in the pSSA generated: while it is true that we did not independently characterize the organic content of our natural seawater sample, it was obtained from a location (Scripps Pier) from which similar samples have been extensively studied in prior lab experiments. Therefore, we have added a sentence and reference to note there was high confidence that the organic content of the pSSA was fairly representative on the basis of a number of prior studies generating SSA from seawater in a MART.

L570-L576: "These two aerosol modes at 100 nm and 800 nm likely represent particles generated from film and jet drops, respectively, consistent with a previous laboratory study that generated aerosol particles from real seawater (Hill et al., 2023). Prather et al., (2013) showed that the fraction of biological particles increased for particles > 1 μm, and can be up to ~20 % of particles > 2 μm. Therefore, this apparent mode of particles ~800 nm may represent additional aerosolized biologic material such as bacteria, gels, and viruses, that may be enriched with organic particles (Hill et al., 2023), would not exist in the ASW, and may explain lower concentrations in the aSSA+SMA generated from ASW compared to SW between 200 nm and 1 μm."

L249-L258: "It is assumed that particles generated from SW contain high fractions of insoluble organic particles or salt particles mixed with organic carbon below 500 nm, similar to previous lab-generated SSA (Prather et al. 2013; Bertram et al. 2018; Kaluarachchi et al. 2022a). In addition, DeMott et al. (2023) showed particle morphologies of laboratory-generated SSA that include organic coatings in the submicron size range, both before and after similar use of an OFR for oxidation studies. The MART was demonstrated to produce substantially similar size distributions and SSA compositions compared to a more natural wave breaking process for bubble bursting (Prather et al., 2013; Stokes et al., 2013), so no bias in organic content in comparison to natural SSA production is expected. During cooling, the RH_w would be low enough such that organic particles or coatings may form a glassy state (Ignatius et al., 2016; Knopf et al., 2018; Koop et al., 2011), as shown by the shaded green region in Figure 2, which represents the glass transition conditions for sucrose (Zobrist et al., 2008)."

We have also added a few sentences to address your concerns about the lack of organic condensation onto the pSSA.

L548-L567: "Although there were higher number concentrations of aSSA+SMA between 200 nm and 1 μm, there was not a discernable shift towards larger sizes, which would be expected after condensation from the gas phase onto the pSSA. In addition, the low concentrations of pSSA would limit condensation of organics in the OFR and would favor new particle formation. The estimated condensation sink timescales were calculated and shown in the supplemental material, indicating that the condensation sink timescale for the nucleation mode aerosols (SMA-only) was ~3 minutes compared to ~11 minutes for the pSSA. Therefore, it is likely the nucleation mode particles scavenged the majority of the condensable material in the OFR and minimized condensation onto the pSSA. However, prior OFR studies for similar pSSA loadings indicated modest increases in organic volume fractions in pSSA as detected by atomic force microscopy (AFM) following similar oxidation exposures using the same OFR (Kaluarachchi et al. 2022b). These changes were accompanied by modifications in particle phase state in the water subsaturated regime, as well as hygroscopicity, for submicron pSSA. DeMott et al. (2023) discussed how similar OFR studies on laboratory generated pSSA led to apparent changes in organic functionalization, at least as determined by AFM for submicron particles. Raman spectroscopy did not detect functional changes following oxidation in that study, but this was inferred to be a consequence of the emphasis on the 1 μm and larger particle regime for the Raman spectroscopic studies, for which organic volume fractions are already quite small and signal to noise becomes an issue. Finally, DeMott et al. (2023) noted that OFR processing of pSSA led to a decrease in INP concentrations by a factor of a few times in the temperature regime >243 K, where heterogeneous ice nucleation has been shown to be initiated by the organic components in very small fractions of pSSA. It has been unknown if this alteration of ice nucleation at higher temperatures translates to impacts at cirrus temperatures. Further, it is also not known whether changes induced by oxidization of the organics present in the pSSA, or the changes in ice nucleating activity due to organics added via condensation or functional alteration might affect the heterogeneous nucleation process that was inferred to be stimulated by crystalline salts at temperatures below 220 K (Patnaude et al., 2021)."

Finally, we have modified our conclusions to note that although the SMA had very inefficient ice nucleating behavior, we also infer that any condensational contributions to the pSSA did not alter the ice nucleating behavior for a number of different possible reasons. We added a few more clear statements in the Conclusions and also modified the Abstract.

L17-L24: "Similarities between freezing behaviors of the pSSA and aSSA+SMA at all temperatures suggest that the contributions of condensed organics onto the pSSA or alteration of functional groups in pSSA via atmospheric aging did not hinder the major heterogeneous ice nucleation process at these cirrus temperatures, which have previously been shown to be dominated by the crystalline salts. Occurrence of 1 % frozen fraction of SMA, generated in the absence of primary SSA, was observed at/near water saturation below 220 K, suggesting it is not an effective INP at cirrus temperatures, similar to findings in the literature for other organic aerosols. Thus, any SMA coatings on the pSSA would only decrease the ice nucleation behavior of pSSA if the organic components were able to significantly delay water uptake of the inorganic salts, and apparently this was not the case."

L782-L804: "There are a few possible reasons for the similar freezing behaviors between these two particle types: 1) the newly formed particles scavenged the majority of condensable material produced in the OFR and only modest amounts of secondary organics condensed to the pSSA, 2) the air stream remained humidified when entering the OFR and the pSSA particles were thus likely in an aqueous state. Whether oxidation of their organic content could proceed in the wetted or partially wetted state, and whether changes to the pSSA organic content would be similar to that observed when processed in a dry crystalline state is unknown, or 3) the addition of SMA coatings to the pSSA and/or alteration of organic components of the pSSA did not alter the crystallization behaviors, nor did they hinder the water uptake by the inorganic salts. Nevertheless, the inclusion of organic material on the pSSA would likely only hinder the heterogeneous nucleation ability that remains dominated by the crystalline salts. Future studies using more realistic or at least slower atmospheric aging processes, such as what may occur in a typical smog chamber, may better represent the possible organic coatings on pSSA. Additionally, oxidation of pSSA at cold temperatures (< 233 K) and after efflorescence may produce different freezing results than this study due to oxidation under different phase states and morphologies."

L114 - If it's important enough to mention that the "grow light was set to a realistic PAR", please state what the radiation flux was.

L173-L175: "The grow light was set to a realistic PAR (photosynthetically active radiation) quantity of ~175 µmol m^{-2} to keep the microorganisms active and not stimulate a bloom."

L124 – You might consider modifying the section title to something like "pSSA, aSSA + SMA, and SMA generation and characterization"

Thank you for your suggestion, we have instead changed the section title to "Aerosol generation and characteristics".

L133 - There are a few commercial and many home-built OFR designs; based on ensuing details in the following sentences and the information provided in Mayer et al. (2020), this is most likely an Aerodyne Potential Aerosol Mass OFR, but this detail should be clarified in the text.

L153-L155: "Using an Aerodyne Potential Aerosol Mass OFR, we examined the impact of atmospheric oxidation on freezing behavior of primary SSA at cirrus temperatures."

L135 – The text states: "The OFR generates […] O_3 and OH radicals […] using two UV lamps at wavelengths λ = 254 nm and λ =184 nm […] at a 90:10 ratio, with 90 % intensity from λ = 254 and 10 %

from λ =184 nm." This is not correct. First, the secondary Hg emission line in ozone-producing UVC lamps is centered at ~185 nm, not 184 nm. Second, and much more important, the ratio of 254 and 185 nm radiation fluxes is not 90:10. As far as I can tell, the OFR was operated with lamp type "GPH436T5L/VH/4P 90/10", which has doped:fused quartz fractions of 90% and 10%, but emits 185 nm radiation at approximately 0.6% of the intensity of the 254 nm radiation (Rowe et al., 2020).

Thank you for pointing out 185 nm, that was a typo and we have changed the text to indicate185 nm and the ratio of lamp intensities as 0.6%.

L196-L199: "The OFR generates high concentrations of O_3 and OH radicals to oxidize particles using two UV lamps at wavelengths λ = 254 nm and λ =185 nm (Mayer et al., 2020). The UV lamp type used in this study was GPH436T5L/VH/4P 90/10, which emits radiation at the 185 nm wavelength at 0.6 % of the intensity of the 254 nm wavelength (Rowe et al., 2020)."

L137 – 7 ppm O_3 does not translate to 4-6 days of equivalent atmospheric OH oxidation. Please specify the corresponding OH exposure, or range of OH exposure(s), and how they were measured or calculated, along with the ambient OH concentration that was assumed to obtain the stated 4-6 days' aging time.

Thank you for the comment. The oxidation potential was misrepresented using the O_3 concentrations instead of OH. We have modified this discussion as shown below.

L199-L204: "The OH exposure in the OFR was calibrated using the change in carbon monoxide (CO) concentrations inside the OFR, at the same temperature and RH conditions as during the experiments. The change in CO versus light intensity of the lamps uses the CO + OH rate coefficient (k_{OH+CO} ~1.48 * 10^{-13} molecules cm^{-3}). The residence time in the OFR was ~2.2 min and the average OH exposure in the experiments was ~6.31 * 10^{11} molecules sec/cm^3 which translated to ~4–6 days of aging under typical atmospheric conditions (OH = 1.5 *10^6 molecules cm^{-3})."

L164-L205 – "It is clear […] cannot be discounted." - this content seems more appropriate to put in Results & Discussion and/or supplement than in Methods.

Thank you for the comment. We have significantly modified this section. The paragraphs on the particle size distributions have been moved to the results section 3.1.

L481-L595: "Data from the SMPS and APS downstream of the OFR were merged into a complete size distribution, as shown in Figure 4 for all experiments. The solid lines indicate aerosols generated from real seawater and the dashed lines are those generated from artificial seawater. For sizes < 200 nm the aSSA+SMA distributions were dominated by secondary particle formation, as indicated by their similarity to the SMA-only experiment. This is consistent with previous work that showed only a small fraction of the submicron aSSA+SMA number distribution generated from a MART originated from the pSSA (Mayer et al., 2020b; Prather et al., 2013). Mayer et al., (2020b) also suggested that new particle nucleation was favored over condensation in the OFR due to the high OH concentrations and fast oxidation rates. The SW size distributions had higher concentrations of aSSA+SMA than the ASW at sizes < 100 nm, which may indicate additional gas phase emissions from the seawater, capable of oxidizing to condensable species. In general, both aSSA+SMA distributions agree with the pSSA distributions at larger sizes. However, the convergence of the distributions occurs at different aerosol diameters for the ASW and SW, ~200 nm and 1 µm for the ASW and SW, respectively. In addition, the higher concentration of aSSA+SMA compared to pSSA from natural SW between 200 nm and 1 µm (Figure 4b) suggests some modification of the pSSA. This could occur through a number of different factors, including gas-phase condensation, changes to the seawater microbial activity altering emissions, or minor changes to particle generation due to surface tension or temperature variations.

Although there were higher number concentrations of aSSA+SMA between 200 nm and 1 μm, there was not a discernable shift towards larger sizes, which would be expected after condensation from the gas phase onto the pSSA. In addition, the low concentrations of pSSA would limit condensation of organics in the OFR and would favor new particle formation. The estimated condensation sink timescales were calculated and shown in the supplemental material, indicating that the condensation sink timescale for the nucleation mode aerosols (SMA-only) was ~3 minutes compared to ~11 minutes for the pSSA. Therefore, it is likely the nucleation mode particles scavenged the majority of the condensable material in the OFR and minimized condensation onto the pSSA. However, prior OFR studies for similar pSSA loadings indicated modest increases in organic volume fractions in pSSA as detected by atomic force microscopy (AFM) following similar oxidation exposures using the same OFR (Kaluarachchi et al. 2022b). These changes were accompanied by modifications in particle phase state in the water subsaturated regime, as well as hygroscopicity, for submicron pSSA. DeMott et al. (2023) discussed how similar OFR studies on laboratory generated pSSA led to apparent changes in organic functionalization, at least as determined by AFM for submicron particles. Raman spectroscopy did not detect functional changes following oxidation in that study, but this was inferred to be a consequence of the emphasis on the 1 μm and larger particle regime for the Raman spectroscopic studies, for which organic volume fractions are already quite small and signal to noise becomes an issue. Finally, DeMott et al. (2023) noted that OFR processing of pSSA led to a decrease in INP concentrations by a factor of a few times in the temperature regime >243 K, where heterogeneous ice nucleation has been shown to be initiated by the organic components in very small fractions of pSSA. It has been unknown if this alteration of ice nucleation at higher temperatures translates to impacts at cirrus temperatures. Further, it is also not known whether changes induced by oxidization of the organics present in the pSSA, or the changes in ice nucleating activity due to organics added via condensation or functional alteration might affect the heterogeneous nucleation process that was inferred to be stimulated by crystalline salts at temperatures below 220 K (Patnaude et al., 2021).
Both pSSA size distributions showed peaks around 100 nm, in agreement with other studies that generated SSA in laboratory settings (Collins et al., 2014; Patnaude et al., 2021; Quinn et al., 2015). However, there was a slight secondary mode at ~800 nm that only occurred during the real seawater experiments (Figure 4b). These two aerosol modes at 100 nm and 800 nm likely represent particles generated from film and jet drops, respectively, consistent with a previous laboratory study that generated aerosol particles from real seawater (Hill et al., 2023). Prather et al. (2013) showed that the fraction of biological particles increases for particles > 1 μm, and can make up to ~20 % for particles > 2 μm. Therefore, this apparent mode for particles ~800 nm may represent additional aerosolized biologic material such as bacteria, gels, and viruses, that may be enriched with organic particles (Hill et al., 2023), and would not exist in the ASW, and may explain lower concentrations in the aSSA+SMA generated from ASW compared to SW between 200 nm and 1 μm. The differences in the ~800 nm mode could also be due to modifications in droplet generation mechanisms, through small differences in temperature, RH, and surfactant content (Stokes et al., 2013).
For the blank (background) tests, in which the MART was filled with only DI water and the OFR was turned on but MART plunging turned off (black line), it was found that there was also secondary particle formation, likely a result of VOCs emitted from the acrylic material of the MART walls. It is likely that the outgassing of acrylic tank materials and subsequent aerosol formation from those compounds in the OFR occurred in all oxidation experiments. The outgassing may have varied with water temperature, which increased throughout each experimental day, and could contribute to some of the differences observed in the aSSA+SMA and SMA-only size distributions. For example, during the pSSA and aSSA+SMA experiments, particle concentrations below 100 nm were higher later in the day due to the warming of the water with time (Figure S2). During the blank test the water was not pre-cooled as in the SW and ASW experiments due to time constraints, which likely led to higher VOC emissions and may explain the high secondary particle concentrations observed during the blank measurements. Hence, the proportion of secondary particles or condensable material formed in the SMA-only and aSSA+SMA cases that was contributed from direct gas-phase emission from the SW and ASW, compared to other organics from the acrylic outgassing, cannot be determined. Future studies will need to probe SMA ice nucleation

by using non-plastic materials. We will nevertheless assume the role of SMA can be interpreted from the ice nucleation experiments, as will be discussed in the subsequent results sections."

We have elected to leave the second paragraph regarding the aerosol phase state where it was. However, this paragraph has been modified as well, as follows.

L242-L401: "The phase state of the particles before entering the CFDC remains uncertain and could affect the heterogeneous nucleating ability of the aerosol population. Several previous studies have analyzed the temperature- and humidity-dependent phase states of NaCl particles, since they are often used as a proxy for SSA. Previous studies have found that the phase state of NaCl after efflorescence depends on the temperature at which efflorescence occurred, with anhydrous NaCl observed for efflorescence temperatures above 273 K (Bartels-Rausch et al., 2021; Koop et al., 2000b; Peckhaus et al., 2016; Wagner et al., 2012). Since the majority of aerosol drying, including the efflorescence of the salt components of pSSA and aSSA+SMA, occurred at room temperature (Figure 2), it is believed the salts would be in the anhydrous form. However, the phase state and morphology of co-emitted organic particles or coatings on the pSSA and aSSA+SMA are less well understood at low temperatures, and the exact structure was uncertain in this study. This is especially difficult to know for the aSSA+SMA particles, due to the exposure to oxidation in the OFR. It is assumed that particles smaller than 200 nm generated from SW contain high fractions of insoluble organic particles or salt particles mixed with organic carbon below 500 nm, similar to previous lab-generated SSA (Bertram et al., 2018; Kaluarachchi et al., 2022a; Prather et al., 2013). In addition, DeMott et al. (2023) showed particle morphologies of laboratory-generated SSA that include organic coatings in the submicron size range, both before and after similar use of an OFR for oxidation studies. The MART was demonstrated to produce substantially similar size distributions and SSA compositions compared to a more natural wave breaking process for bubble bursting (Prather et al., 2013; Stokes et al., 2013), so no bias in organic content in comparison to natural SSA production is expected. During cooling, the RHw would be low enough such that organic particles or coatings may form a glassy state (Ignatius et al., 2016; Knopf et al., 2018; Koop et al., 2011), as shown by the shaded green region in Figure 2, which represents the glass transition conditions for sucrose (Zobrist et al., 2008)."
Aerosols that contain organic material may either enhance heterogeneous nucleation (Wilson et al., 2012) or have no effect (Kasparoglu et al., 2022). For example, organic coatings on mineral dust particles have been shown to suppress heterogeneous nucleation toward higher RH at cirrus temperatures (Möhler et al., 2008), depending also on the coating thickness or the fractional coverage of the particles, while another study found organic coatings on mineral dust had no effect on immersion freezing between 253–233 K regardless of the coating thickness (Kanji et al., 2019). At warmer temperatures > 233 K, organic coatings may be in a less viscous or liquid-like phase state, while at colder temperature may become semi-solid or glassy (Charnawskas et al., 2017), which may explain the differences in ice nucleation behavior of particles with organic coatings in those studies. Specifically, the inclusion of glassy coatings on the pSSA or aSSA+SMA particles may inhibit water uptake and delay dissolution of the salt components until higher RH_w is reached."

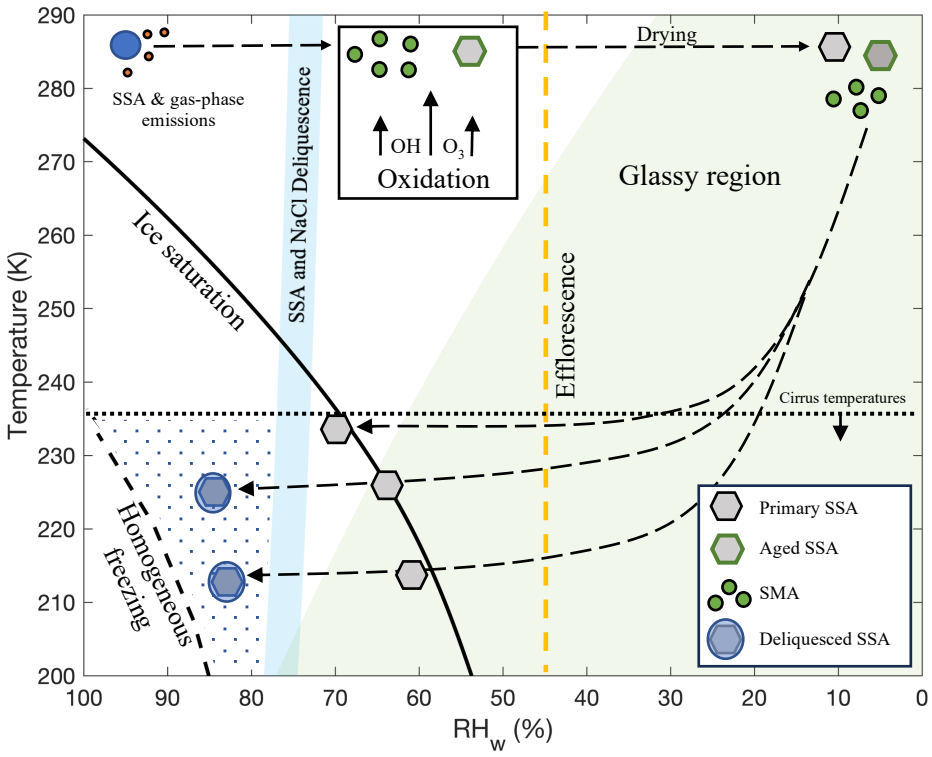

Figure 2. Expected trajectory and phase state of the pSSA, aSSA+SMA and SMA particles for CFDC experiments, modified from Patnaude et al. (2021). Orange dashed line is the expected efflorescence line for NaCl on the basis of the parametrization of anhydrous NaCl and extrapolated to cirrus temperatures (Tang & Munkelwitz, 1993). The blue shaded region represents the range of possible deliquescence RHs for NaCl and SSA, using the parameterization from Tang & Munkelwitz, (1993) for NaCl extrapolated to colder temperatures as the upper bound and shifting it down 4 % RH for SSA similar to Wagner et al. (2018). The long dashed black lines follow the path of aerosol particles as through drying, cooling, and CFDC scans at different temperatures. The blue circles represent aqueous solutions, gray hexagons represent effloresced pSSA aerosols, and the light blue circles with embedded hexagons represent fully deliquesced particles. The gray hexagons with green outlines and green circles represent the aSSA+SMA and SMA particles, respectively. Lines indicating ice saturation and predicted homogeneous freezing conditions are also denoted. The dotted region represents conditions where aerosol particles experience ice supersaturated conditions and relative humidities that exceed their deliquescence point. The green shaded region represents conditions below the glass transition curve of sucrose from Zobrist et al. (2008).

L171 – I strongly disagree that these factors alone enhance nucleation. While the gas-phase oxidation rate was indeed accelerated with the use of elevated OH concentrations, gas-to-particle condensation rates could in principle also have been increased by using SSA concentrations and increasing the condensation sink. Since pSSA concentrations were only 140 cm^{-3}, (L306), which is far lower than even seed particle concentrations used in many environmental chamber studies with OH concentrations that are closer to atmospheric OH concentrations, it seems to be me that homogenous nucleation of SMA particles was just as likely (if not more likely) due to the very low pSSA condensation sink than the high oxidant concentrations.

We agree with this analysis. Please see response to the first comment about condensation vs. new particle formation.

L181 - what exactly constitutes a "blank" or "background" experiment in this context? MART air sampled through the OFR with in the absence of pSSA generation? This was not clear to me.

The blank experiments were intended to resemble the SMA experiments, where the OFR was turned on but the MART plunging was turned off. Therefore, it was only the MART headspace air that was being sampled. The main difference was for the blank experiment, the MART was filled with DI water. We have modified the sentence to make this clearer.

L578-L580: "For the blank (background) tests, in which the MART was filled with only DI water and the OFR was turned on but MART plunging turned off (black line), it was found that there was also secondary particle formation, likely a result of VOCs emitted from the acrylic material of the MART walls."

L265-L270: "In these experiments […] the cycle was repeated" – this content seems more appropriate to put in Methods. It would also be useful to explain why 10% and 0.1% frozen fractions were chosen as the benchmark conditions for ending and beginning the RH scans in the CFDC.

We moved those sentences to section 2.3 per this recommendation and added a few sentences as to why the ice fraction thresholds were chosen and why we believe they are appropriate for this study.

L421-L429: "The thresholds of ice fraction for the RH_w scans required 10 continuous seconds above 10 % or below 0.1 % in order to reset the scans. Note these activated fractions were calculated based on particle counts in channels above a selected OPC channel to define ice counts during the experiments, as opposed to the more accurate method for calculation of ice fraction that accounted for the background aerosol distribution (described below). Using 10 % and 0.1 % as endpoints of the RH_w scans resulted in a broad range in RHs being covered. By the time 10 % of the particles had nucleated, the RH_w was at above homogeneous freezing conditions (Koop et al., 2000a) and it was not necessary to continue raising the RH_w. The lower threshold of 0.1 % for 10 continuous seconds was sufficient to reset the scans as the RH_w was then well below the deliquescence RH_w for NaCl and SSA (~74 %; Tang and Munkelwitz, (1993)), with the exception of RH_w at warmer temperatures > 225 K, where the RH_w scans did not reach below ~75 % but we did not expect heterogeneous freezing conditions."

L271/Figure 4: Figure 4a is confusing - I don't understand why heterogenous freezing occurs over the first 3 CFDC scans and homogenous freezing occurs over the last 3 CFDC scans for what I assume is nominally the same pSSA. Also, the "Temperature" axis/label is too vague; if I understand Figure 4 correctly, only T_ow is being shown, whereas T_rw is not. Please update the figure axis/legend to clarify this either way.

The temperature is the column temperature. The reason it rises slightly is due to the T_{OW} increasing. We have modified this figure to make it easier to see the differences in the particles freezing and the RH conditions where this occurred, and added some more descriptive sentences to make this clearer. As explained in the modified text below, a gradual increase in ice particle counts is indicative of heterogeneous freezing, whereas homogeneous freezing is associated with a more abrupt change at a specific RH_w.

L597-L604: "Figure 5a shows a time series of CFDC scans for a pSSA experiment. The first three scans, which occurred below 220 K showed a gradual increase in ice particle counts (light blue markers) with increasing RH_w, starting around 65 %. The final three scans beginning ~218 K, showed a more modest increase in ice particle counts until the RH_w reached nearly 100 %, resulting in a very sharp increase in ice particle counts. The first three scans indicate particles freezing via heterogeneous nucleation due to the slow and gradual increase of ice particles, with the initial formation of ice particles below 75 % RH_w. In

contrast, the last three scans showed very few ice particles below 85 % RH_w, but then had a sudden and dramatic spike in ice particles when the RH_w was > 90 %. The fourth scan may be at/near the transition between the two freezing mechanisms, as there were some increased ice particle counts at RH_w < 80 %, but we also observed the sharp spike in ice particles when the RH_w was near water saturation."

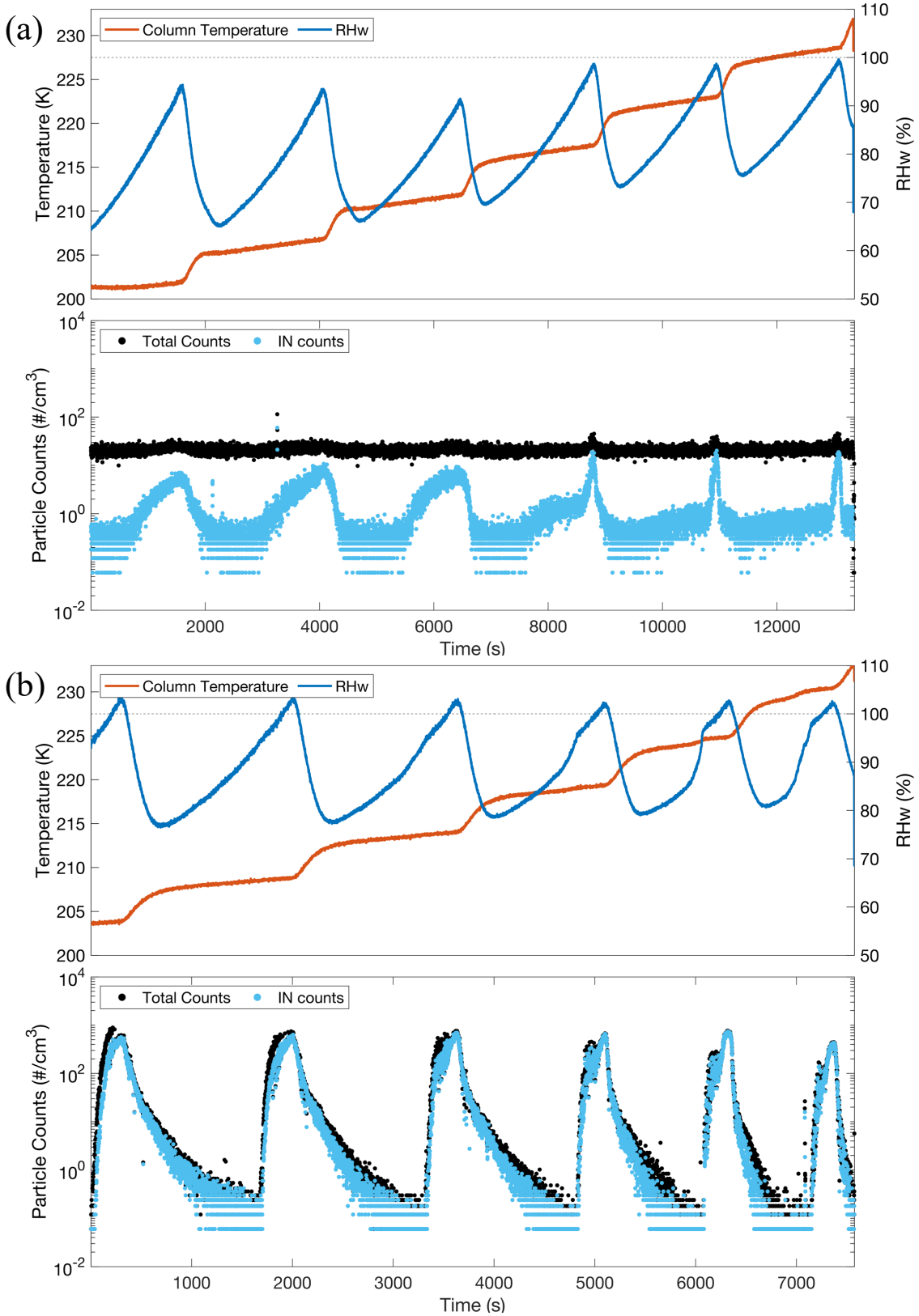

Figure 5. Time series of CFDC scans for (a) pSSA and (b) SMA experiments generated from real seawater beginning at 204 K. The CFDC column temperature is represented by the red lines, and the blue lines represents the RH_w. The black and light blue markers indicate the numbers of total particles counted in the

OPC and those that are considered ice crystals, respectively. The black dotted horizontal lines in the top panels of (a) and (b) represent water saturation.

L278: What exactly is the "expected homogeneous freezing threshold?"

Threshold was probably a poor choice of wording. Instead, we have changed this sentence to make this clearer.

L609-L611: "These cases illustrate that SMA froze through a homogeneous freezing mechanism, as there was almost no ice formed until the RH_w exceeded conditions expected for homogeneous freezing (Koop et al., 2000a)."

L283/Figure 5: why are 1% and 5% frozen fractions shown here, whereas the 10% frozen fraction was used as the RH scan endpoint earlier (Fig. 4)? The presentation of multiple frozen fraction values without explanation for the underlying reasons comes across as confusing/arbitrary.

See our earlier response as to why the 0.1 and 10 % activation fractions were used. These activation fractions (0.1 % and 10 %) were simply used as automated scan endpoint thresholds to provide a range of RHs for each temperature. Our more accurate method for calculation of ice fraction was only used to determine the 1 % and 5 % ice fraction for presentation. When using the more accurate method described in section 2.3, we did not find observations of 10 % ice fraction. We have added the following to explain.

L620-L621: "Note when using this method, 10 % ice fraction was no longer observed in any of the experiments and is the reason for presentation of 5 % instead."

References

Bertram, T. H., Cochran, R. E., Grassian, V. H. and Stone, E. A.: Sea spray aerosol chemical composition: Elemental and molecular mimics for laboratory studies of heterogeneous and multiphase reactions, Chem. Soc. Rev., 47(7), 2374–2400, doi:10.1039/c7cs00008a, 2018.

Charnawskas, J. C., Alpert, P. A., Lambe, A. T., Berkemeier, T., O'Brien, R. E., Massoli, P., Onasch, T. B., Shiraiwa, M., Moffet, R. C., Gilles, M. K., Davidovits, P., Worsnop, D. R. and Knopf, D. A.: Condensed-phase biogenic–anthropogenic interactions with implications for cold cloud formation, Faraday Discuss., 200, 165–194, doi:10.1039/C7FD00010C, 2017.

DeMott, P. J., Hill, T. C. J., Moore, K. A., Perkins, R. J., Mael, L. E., Busse, H. L., Lee, H., Kaluarachchi, C. P., Mayer, K. J., Sauer, J. S., Mitts, B. A., Tivanski, A. V, Grassian, V. H., Cappa, C. D., Bertram, T. H. and Prather, K. A.: Atmospheric oxidation impact on sea spray produced ice nucleating particles, Environ. Sci. Atmos., doi:10.1039/d3ea00060e, 2023.

Ignatius, K., Kristensen, T. B., Järvinen, E., Nichman, L., Fuchs, C., Gordon, H., Herenz, P., Hoyle, C. R., Duplissy, J., Garimella, S., Dias, A., Frege, C., Höppel, N., Tröstl, J., Wagner, R., Yan, C., Amorim, A., Baltensperger, U., Curtius, J., Donahue, N. M., Gallagher, M. W., Kirkby, J., Kulmala, M., Möhler, O., Saathoff, H., Schnaiter, M., Tomé, A., Virtanen, A., Worsnop, D. and Stratmann, F.: Heterogeneous ice nucleation of viscous secondary organic aerosol produced from ozonolysis of α-pinene, Atmos. Chem. Phys., 16(10), 6495–6509, doi:10.5194/acp-16-6495-2016, 2016.

Hill, T. C. J., Malfatti, F., McCluskey, C. S., Schill, G. P., Santander, M. V., Moore, K. A., Rauker, A. M., Perkins, R. J., Celussi, M., Levin, E. J. T., Suski, K. J., Cornwell, G. C., Lee, C., Del Negro, P., Kreidenweis, S. M., Prather, K. A. and DeMott, P. J.: Resolving the controls over the production and

emission of ice-nucleating particles in sea spray, Environ. Sci. Atmos., 3(6), 970–990, doi:10.1039/D2EA00154C, 2023.

Kaluarachchi, C. P., Or, V. W., Lan, Y., Madawala, C. K., Hasenecz, E. S., Crocker, D. R., Morris, C. K., Lee, H. D., Mayer, K. J., Sauer, J. S., Lee, C., Dorce, G., Malfatti, F., Stone, E. A., Cappa, C. D., Grassian, V. H., Prather, K. A. and Tivanski, A. V.: Size-Dependent Morphology, Composition, Phase State, and Water Uptake of Nascent Submicrometer Sea Spray Aerosols during a Phytoplankton Bloom, ACS Earth Sp. Chem., 6(1), 116–130, doi:10.1021/acsearthspacechem.1c00306, 2022a.

Kaluarachchi, C. P., Or, V. W., Lan, Y., Hasenecz, E. S., Kim, D., Madawala, C. K., Dorcé, G. P., Mayer, K. J., Sauer, J. S., Lee, C., Cappa, C. D., Bertram, T. H., Stone, E. A., Prather, K. A., Grassian, V. H. and Tivanski, A. V.: Effects of Atmospheric Aging Processes on Nascent Sea Spray Aerosol Physicochemical Properties, ACS Earth Sp. Chem., 6(11), 2732–2744, doi:10.1021/acsearthspacechem.2c00258, 2022b

Knopf, D. A., Alpert, P. A. and Wang, B.: The Role of Organic Aerosol in Atmospheric Ice Nucleation: A Review, ACS Earth Sp. Chem., 2(3), 168–202, doi:10.1021/acsearthspacechem.7b00120, 2018.

Koop, T., Bookhold, J., Shiraiwa, M. and Pöschl, U.: Glass transition and phase state of organic compounds: dependency on molecular properties and implications for secondary organic aerosols in the atmosphere, Phys. Chem. Chem. Phys., 13(43), 19238, doi:10.1039/c1cp22617g, 2011.

Rowe, J. P., Lambe, A. T., and Brune, W. H.: Technical Note: Effect of varying the λ = 185 and 254 nm photon flux ratio on radical generation in oxidation flow reactors, Atmos. Chem. Phys., 20, 13417–13424, https://doi.org/10.5194/acp-20-13417-2020, 2020.